Available online at www.sciencedirect.com
SCIENCE DIRECT
Journal of Molecular Catalysis A: Chemical 249 (2006) 191–200
JOURNAL OF MOLECULAR CATALYSIS A: CHEMICAL
www.elsevier.com/locate/molcata

Hydrogen adsorption on a $Mo_{27}S_{54}$ cluster: A density functional theory study

Xiao-Dong Wen [a], Tao Zeng [a], Bo-Tao Teng [a], Fu-Qiang Zhang [a], Yong-Wang Li [a], Jianguo Wang [a], Haijun Jiao [a,b,*]

[a] *State Key Laboratory of Coal Conversion, Institute of Coal Chemistry, Chinese Academy of Sciences, Taiyuan, Shanxi 030001, PR China*
[b] *Leibniz-Institut für Katalyse e.V. an der Universität Rostock, Albert-Einstein-Strasse 29a, 18059 Rostock, Germany*

Received 14 June 2005; received in revised form 7 January 2006; accepted 10 January 2006
Available online 14 February 2006

Abstract

Density functional theory computations have been carried on the hydrogen adsorption mechanism on a $Mo_{27}S_{54}$ single layer cluster, which has a size (15–20 Å) close to that of real catalysts. For one molecule of H_2 adsorption, the most stable adsorption form ($E_{ads} = -27.2$ kcal/mol) is the homolytic dissociation on the S edge with the hydrogen atoms keeping away from the plane consisting of all Mo atoms, followed by the heterolytic dissociation ($E_{ads} = -26.1$ kcal/mol) on the intersection of S and Mo edges with the formation of Mo_c–H and S_c–H bonds. At high coverage with two and three H_2, however, dissociated hydrogen adsorption on the Mo sites are much more favored thermodynamically than on the S sites. Moreover, the corner sites are more favored thermodynamically for hydrogen adsorption and formation of coordinatively unsaturated sites than the edge sites. In addition, the activation energy of H_2 dissociation and hydrogen transfer processes have been computed to be 2.7–19.2 kcal/mol, and these rather low barriers indicate the enhanced mobility of the adsorbed hydrogen on the surface.

Keywords: DFT; Hydrogen Adsorption; MoS_x; Catalysis

1. Introduction

During the last decades lots of efforts have been devoted to the understanding of the MoS_2 active sites for hydrodesulfurization (HDS) and hydrogenation (HYD) [1–5]. Hydrogen species on the surfaces of catalysts is crucial to catalytic activity. In the "remote-control" model, Delmon et al. have proposed two distinct sulfide phases (Co_9S_8 and MoS_2) on the Co promoted MoS_2 catalyst for thiophene HDS, and the catalytic activity is ascribed to the surface –SH, which can be enriched by activated hydrogen over Co_9S_8 (hydrogen spillover). The activated hydrogen species forms not only surface –SH for hydrogenolysis of sulfur containing compounds [6–9] but also remove surface sulfur to maintain an effective degree of coordinately unsaturated sites (CUS) on MoS_2. It has been proven experimentally that properly reduced MoS_2 edges have unique activities for HDS and HYD [1,3,6]. However, the detailed mechanism of formation and exact structures of the active sites still remain unclear, and they continue to be the subject of investigations in many aspects [2,3,9].

It is well known that MoS_2 consumes large quantities of H_2 [10–12], but the dissociation process of H_2 and the states of the adsorbed hydrogen on MoS_2 are unclear. Two H_2 dissociation schemes, i.e.; heterolytic dissociation on sulfur vacancies to yield Mo–H and Mo–SH species, and homolytic dissociation on disulfide groups to form Mo–SH groups, have been considered [11,13]. The latter process has been observed on molecular coordinated complexes [14].

Raman spectroscopy and X-ray photoelectron spectroscopy studies on MoS_2-based systems have detected disulfide species [11,15–17] and –SH groups [10,18–20], but no Mo–H species has been found, and infrared studies have shown the location of –SH groups at the MoS_2 edges [19]. The –SH groups have been directly observed by inelastic neutron scattering by Wright et al. [10] and Sundberg et al. [21] on bulky and Al_2O_3 supported MoS_2, and a spectral peak at ca. 600 cm^{-1} has been assigned to the Mo–S–H deformation mode. Other spectroscopic studies have only evidenced –SH groups indirectly. On the basis of the

* Corresponding author.
E-mail address: haijun.jiao@ifok-rostock.de (H. Jiao).

1381-1169/$ – see front matter © 2006 Elsevier B.V. All rights reserved.
doi:10.1016/j.molcata.2006.01.018

infrared spectra of (Co)Mo/Al_2O_3 catalysts, Topsøe et al. have observed the hydrogen bonding interaction between the –OH groups on the support and the acidic –SH groups [22], and shown the enhanced acidity of –SH group by using pyridine as a probe molecule [19]. Recently, Maugé et al. have shown an increase in the Brønsted acidity of –SH groups by H_2S adsorption, compared to the sulfide phase on similar catalytic systems [23–25], Lauritsen et al. have observed in scanning tunneling microscopy experiment the formation of –SH groups on the edges of MoS_2 nanocluster [26,27]. On the unsupported and supported catalysts Thomas et al. [28–31] and Hensen et al. [32] have observed the heterolytic dissociation of H_2, as indicated by the exchanges of H_2/D_2 and H_2S/D_2S. This shows the importance of the mobility of hydrogen species on the surface. Since the catalytic HDS activity depends on the types of CUS, it is necessary to understand the adsorbed hydrogen on the catalyst surface. CUS is formed by the removal of surface sulfur by activated hydrogen, and therefore, the higher the concentration of activated hydrogen, the higher the CUS concentration, and the higher the HDS activity. Despite the extensive experimental studies, however, the detailed mechanism of formation and exact structures of the active CUS still remain unclear, and they continue to be the subject of investigations in many aspects.

In addition to experiments, theoretical studies have shown the heterolytic dissociation of H_2 on the surfaces of metal sulfides (MoS_2, NiS_x and RuS_2) [13,33,34] with the formation of metal hydrides and –SH groups. On the basis of periodic density functional theory study on H_2 adsorption on MoS_2, Cristol et al. have found that the most stable surface does not contain any CUS, and that the heterolytic dissociation of H_2 forming Mo–H and –SH is always endothermic without formation of new CUS on the surface [35]. Travert et al. also have found the ability to dissociate H_2 on the surface depending on the nature of metal atom and the sulfur coordination environment [36]. Byskov et al. have studied the dissociation of H_2 on the edges of a Co promoted MoS_2 slab, and found that sulfur atoms at the edges of the MoS_2 slabs can move up to extract one hydrogen atom from the dissociating H_2 and transport it to the other side of the slab where it diffuses on [37]. Also using a periodic model, Bollinger et al. [38] studied the electronic structures of MoS_2 nano-particles, and the hydrogen adsorption on the Mo and S edges. It is found that hydrogen adsorption on the S edge with the formation of two –SH groups represents the most stable conformation, and that on the Mo edge is also possible with half S coverage on it. On the basis of calculated free energy including H_2 and H_2S, Bollinger et al. found that hydrogen is expected to be adsorbed at both the Mo and S edges in the form of –SH groups under HDS conditions, and concluded that the availability of activated hydrogen is an important prerequisite for the HDS process. Li et al. have discussed the effect of removal of sulfur atoms from Mo_7S_{24} edges for understanding the activation mechanisms of HDS/HYD catalysts [39]. Paul and Payen have studied the vacancy formation mechanism on the edges of MoS_2 nano-crystallites as active phases in HDS process, and the dynamic equilibrium on these edges [40]. From the thermodynamic point of view, the formation of vacancies on the edges of the MoS_2 nano-crystallites is an unfavorable process. The results of catalytic testing and kinetic study have proven that the reduced edges of the highly dispersed MoS_2 crystals with a size of one to several nanometers with boundaries in all crystallographic directions provide the necessary active sites for the HDS/HYD reactions [1–4,41–44]. The data of the extended X-ray adsorption spectroscopy and scanning tunneling microscopy showed that the boundaries of MoS_2 were more relaxed [26,45,46].

The present work reports a detailed approach to explore H_2 adsorption and activation on the $Mo_{27}S_{54}$ cluster by using the density functional theory method. The vibrational frequencies of –SH and Mo–H groups are computed and compared with the available experimental data. The transfer of activated hydrogen (spillover hydrogen) and the role of hydrogen in the formation of CUS are discussed. The reactivity of activated hydrogen with different sulfur atoms on the edges of $Mo_{27}S_{54}$ is analyzed to understand the HDS catalytic nature on MoS_2.

2. Method and model

All calculations are performed with the program package DMol^3 in the Materials Studio 2.2 of Accelrys Inc. In DMol^3 the physical wave functions are expanded in terms of accurate numerical basis sets [47]. We have used the doubled numerical basis set with p-polarization function for hydrogen and d-polarization functions for other atoms (DNP), while effective core potential (ECP) is used for molybdenum. The generalized gradient corrected functional by Perdew and Wang (PW91) is employed [48], and the medium quality mesh size is used for the numerical integration. The tolerances of energy, gradient, and displacement convergence are 2×10^{-5}, 4×10^{-3} au/Å, 5×10^{-3} Å, respectively. The real space cutoff of atomic orbitals is set at 5.5 Å, and a Fermi smearing of 0.0005 was used to count the orbital occupancy. The Linear Synchronous Transit/Quadratic Synchronous Transit method at the same level is used for the search for transition states.

In order to model the nanometer sized crystallites observed experimentally, a $Mo_{27}S_{54}$ cluster is used, and the initial coordinates are taken from the handbook of crystal structures; this cluster has also been used by Li et al. [49] and Orita et al. [50] to study the structural and electronic properties of MoS_2. It is to be noted that the highly dispersed supported MoS_2 catalysts have predominant sizes in the range of 10–30 Å [51]. This indicates that there should be two, three, or four Mo atoms on a corresponding edge plane and that the electronic properties of Mo atoms at different positions (corner or edge sites) of the edge planes should be different [52]. Recently, theoretical studies on CO adsorption show that $Mo_{16}S_x$ and $Mo_{20}S_x$ clusters are large enough to represent both stoichiometric and non-stoichiometric cluster models [53,54]. Further calculations on the surface structures and stability show that $Mo_{16}S_x$ and $Mo_{19}S_x$ clusters on Mo sites, and $Mo_{18}S_x$ cluster on S site are realistic models for studying H_2 adsorption and activation [55]. Therefore, the use of $Mo_{27}S_{54}$ cluster with size close to real MoS_2 particles should be reasonable and realistic.

However, the adsorption of H_2 on $Mo_{27}S_{54}$ still remains unclear. We have optimized the cluster by using our methods, as shown in Fig. 1. This finite slab represents $(\bar{1}\,0\,1\,0)$ for the

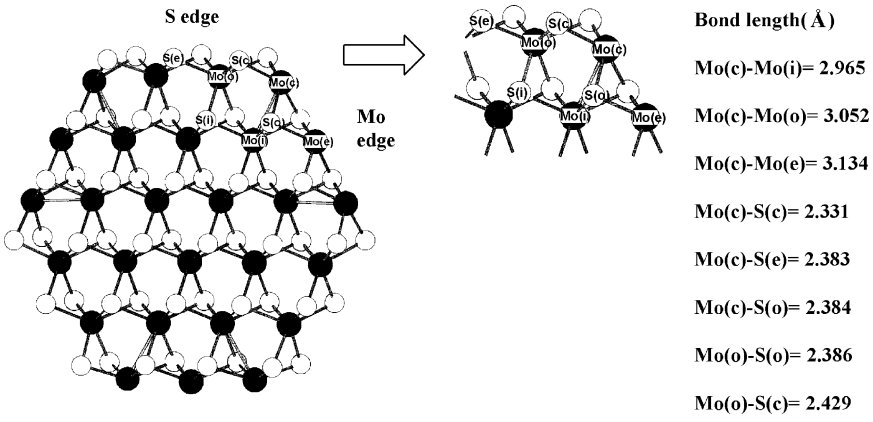

Fig. 1. Optimized structure parameters for $Mo_{27}S_{54}$ with the S and Mo edges for adsorption H_2.

S edge and $(1\,0\,\bar{1}\,0)$ for the Mo edge of MoS_2. Due to its D_{3h} symmetry, there are two types of bridge sulfurs (S_c and S_e) on the S edge, and two types of molybdenum centers (Mo_c and Mo_e) on the Mo edge, respectively. To validate the method in DMol, we have compared the optimized structural parameters of our $Mo_{27}S_{54}$ cluster with those from the EXAFS data [56] and those from DFT based calculation with the Vienna Ab Initio Simulation Program (VASP) [35]. The characteristic distances of the bulk structure (d1) and those (d2 and d3) of neighboring molybdenum atoms at the two types of edge estimated from our calculation (3.16, 3.08 and 3.25 Å) agree well with the available EXAFS (3.16, 3.32 and 3.32 Å) and VASP data (3.16, 3.12 and 3.22 Å).

In this work, both dissociative and non-dissociative adsorptions of H_2 molecule on the Mo edge and on the S edge have been calculated. In addition, we also have calculated the frequencies of S–H and Mo–H groups using the partial Hessian matrix including only atoms of S–H, Mo–H to reduce the computational cost. Indeed, this approximation has been found reasonable on the basis of the identical CO stretching frequencies computed for adsorbed CO on MoS_x from the matrix corresponding to all CO and surface atoms and from matrix corresponding only to CO, indicating that surface atom does not influence CO stretching at all [55]. Comparison of the experimental and calculated stretching frequency for H_2 (expt. 4401 cm^{-1} and calc. 4369 cm^{-1}) gives a ratio of 1.01, which is used to scale other frequencies. In addition, the possible CUS on the S edge and the migration of hydrogen are discussed. From these results, we can propose the mechanism of creating CUS over MoS_2 cluster. Adsorption energies are computed by subtracting the energies of the gas-phase H_2 and cluster from the energy of the optimized H_2/cluster complex; n is the number of adsorbed H_2, as shown in Eq. (1). On this basis, the more negative the E_{ads}, the stronger the adsorption. Energetic data are listed in Table 1:

$$E_{ads} = E(nH_2/Mo_{27}S_{54}) - [En(H_2) + E(Mo_{27}S_{54})] \quad (1)$$

3. Results and discussion

3.1. Adsorption at low hydrogen coverage

3.1.1. Adsorption on the Mo edge

Fig. 2 shows four different adsorption structures (**1**–**4**) of H_2 on the Mo edge. In **1** and **2**, H_2 is located germinally at Mo_c with the Mo–H bond lengths of 1.886/1.896 and 1.873/1.866 Å, and the H–H bond length of 0.854 and 0.878 Å, respectively. This shows that the adsorbed H_2 is activated but not dissociated, and represents the initial point for H_2 dissociation. In **3**, there are one Mo–H–Mo bridge group (Mo–H = 1.902–1.924 Å) and one terminal Mo–H group (Mo–H = 1.732 Å), while there are

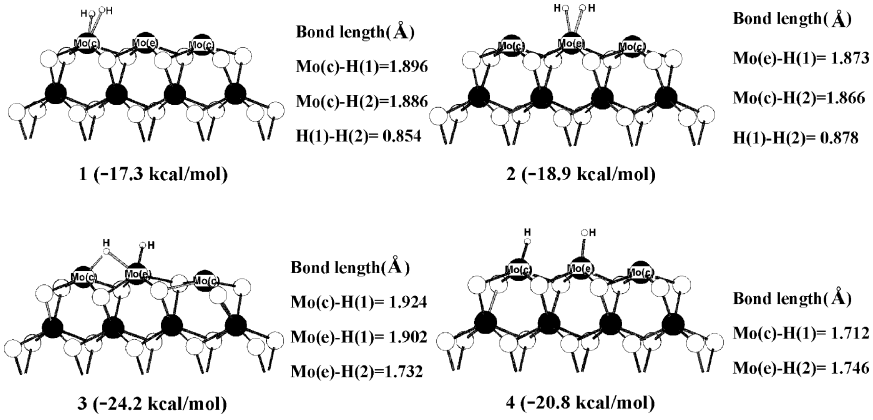

Fig. 2. The stable H_2 adsorption modes (**1**–**4**) and adsorption energies on the Mo edge.

Table 1
Calculated total electronic energies (E_{tot}, au), the relative energies (E_{rel}, kcal/mol) and the adsorption energies (E_{ads}, kcal/mol)

Model	E_{tot}	E_{rel}	E_{ads}[a]
1	−23355.06760	9.9	−17.3
2	−23355.07011	8.3	−18.9
3	−23355.07866	3.0	−24.2
4	−23355.07321	6.5	−20.8
5	−23355.06055	14.3	−12.9
6	−23355.05409	18.4	−8.8
7	−23355.08166	1.2	−26.1
8	−23355.08335	0.0	−27.2
9	−23355.07856	3.0	−24.2
10	−23355.07239	6.9	−20.3
11	−23355.07035	8.1	−19.1
12	−23355.06840	9.5	−17.8
13	−23355.05840	15.7	−11.5
14	−23355.05253	19.4	−7.8
15	−23355.05009	21.0	−6.2
16	−23355.04612	23.3	−3.9
17	−23355.01236	44.5	17.3
18	−23357.45080	[22.8][b]	−43.8
19	−23357.48727	[0.0][b]	−66.6
20	−23356.26043	(12.9)[c]	−31.4
21	−23356.25897	(14.1)[c]	−30.2
22	−23356.28124	(0.0)[c]	−44.3
23	−23356.28091	(0.2)[c]	−44.0
24	−23356.27749	(2.3)[c]	−42.0
25	−23357.44091	[29.1][b]	−37.6
26	−23356.26398	(10.8)[c]	−33.4
27	−23356.25009	(19.4)[c]	−24.9
28	−23357.42418	[39.7][b]	−27.0
29	−23356.25153	(18.7)[c]	−25.6
30	−23356.24030	(25.6)[c]	−18.7
31	−23355.02841	–	–
32	−23355.02505	–	–
33	−22955.63610	–	–
34	−22955.61168	–	–
TS(1) (2 → 3)	−23355.06021		
TS(2) (4 → 3)	−23355.06030		
TS(3) (1 → 7)	−23355.04739		
TS(4) (5 → 7)	−23355.03348		
TS(5) (5 → 16)	−23355.03006		
TS(6) (16 → 11)	−23355.04173		
TS(7) (14 → 11)	−23355.04386		
TS(6) (6 → 14)	−23355.03304		
$Mo_{27}S_{54}$	−23353.86943		
H	−0.50141		
H_2	−1.17057		
H_2S	−399.40282		

[a] According to Eq. (1).
[b] For six hydrogen atoms.
[c] For four hydrogen atoms.

two terminal Mo–H groups in **4** (Mo–H = 1.712 and 1.746 Å), respectively. They represent homolytic adsorption of H_2 on the Mo edge.

As given in Table 1, the adsorption of dissociated hydrogen is more favored thermodynamically than the activated H_2, as indicated by the computed adsorption energies (−24.2/−20.8 kcal/mol versus −18.9/−17.3 kcal/mol, respectively). It also shows that the adsorption of dissociated hydrogen favors **3**, which is also the most stable structure for hydrogen on the Mo edge. It is to be noted that the adsorption energy (−24.2 kcal/mol) of **3** is close to the experimental value of −28.8 to −24.9 kcal/mol on Mo surface obtained by Farias et al. [57]. The most stable activated H_2 complex is **2**, which is 5.3 kcal/mol higher in energy than **3**, and this energetic difference is much smaller than the dissociation energy of H_2 by 104.2 kcal/mol [58], indicating the considerable activation of H_2 in **2** and the enhanced stabilization of atomic hydrogen in **3**. On the basis of the calculated relative energies, it is interesting to note that structure **2** should be the initial point for H_2 activation, and that the adsorbed H_2 complex will dissociate oxidatively into the dihydride complex (**3**) with the shift of one hydrogen to the bridge position, while **4** and **1** should be the higher energetic intermediates for H_2 adsorption and hydrogen transfer.

3.1.2. Adsorption on the S edge

In addition to the adsorption on the Mo edge, we calculated the possible adsorption on the S edge. As shown in Fig. 3, there are four structures (**5**–**8**) for hydrogen adsorption on the S edge, and **5**, **6** and **8** represent the homolytically dissociated hydrogen at S_c and S_e bridges, while **7** shows the heterolytically dissociated hydrogen.

In **5** and **6**, the S_c–H and S_e–H bond lengths are 1.361 and 1.357 Å, and the Mo_c–S_c and Mo_e–S_e distances are 2.490 and 2.509 Å, respectively, which are longer than those in the bare surface (2.331 and 2.383 Å). In **7**, the S_c–H_2 and Mo_c–H_1 bond lengths are 1.356 and 1.726 Å. For **8**, the two S–H groups with the corner and edge on the same side have bond lengths of 1.367 and 1.366 Å, respectively.

The computed relative energies in Table 1 identify **8** as the most stable form, and the second most stable form is **7**, which is higher in energy than **8** by only 1.2 kcal/mol. In contrast, other structures (**1**–**6**) are higher in energy. The most stable form **8** has also the largest adsorption energy of −27.2 kcal/mol, while that of **7** is −26.1 kcal/mol. These results agree very well with those from periodic conditions by using other theoretical models and methods. For example, Cristol et al. [35] found that the most stable adsorption geometry on the S edge has two –SH groups, and that the adsorption energy is −31.8 kcal/mol. Bollinger et al. [38] have found that hydrogen adsorption on the top of the fully covered S edge with the formation of two –SH groups is the most stable configuration, and the adsorption energy is −29.1 kcal/mol. It is to be noted that our most stable adsorption model (**8**) has the same adsorption configuration as the two most stable models from the periodic calculations. This validates not only our cluster model but also the methods employed. Therefore, there are no fundamental difference between our cluster model and periodic model for hydrogen adsorption on the S edge.

At this step, it is very interesting to compare the relative energies for H_2 adsorption at both S and Mo edges. As shown in Table 1, structure **8** is the most stable species with one S_e–H and one S_c–H on the S edge, and structure **7** is the second most stable species with one S–H and one Mo–H bonds around the corner of one CUS at Mo, which represents the intersection of molybdenum and sulfur edges. The third most stable adsorption form is structure **3** with one Mo–H–Mo bridge group and one terminal Mo–H bond. This small energetic difference of 1.2 kcal/mol

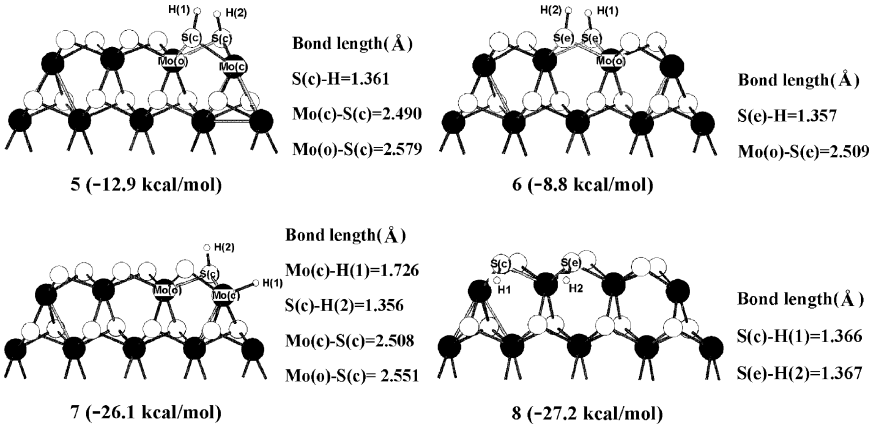

Fig. 3. H_2 dissociation adsorption modes (**5**–**8**) and adsorption energies on the S edge.

between **7** and **8** indicates the possibility of co-existence of both forms from homolytic and heterolytic hydrogen adsorption on the basis of thermodynamic consideration. Indeed, Hall et al. have reported that heterolytic chemisorptions afford the best rationalization of the experimental catalysis data [59]. On the basis of this small energy difference one can consider that the adsorbed hydrogen can migrate easily from one CUS to another CUS to archive the most stable adsorption with rather low barrier, as discussed below.

For comparison, we have calculated other structural isomers with two –SH groups on the S edge. The optimized structures are given in Fig. 4, and the energetic data are listed in Table 1. It shows clearly that structure **9** with two bridging –SH groups is only 3.0 kcal/mol higher in energy than **8**, and this is only due to the different orientations of the –SH group at S_e, while other structures (**9**–**13**) are much higher in energy. In addition, we have computed structures with one –SH and one –MoH groups (**14**–**16**) or with two –MoH groups (**17**) on the sulfur edge, and they are higher in energy. The calculated adsorption energy (Table 1) shows that on the sulfur edge structures with two –SH groups or one –SH group and one –MoH group are exothermic, while structure **17** with two –MoH groups is endothermic. This is in sharp contrast to the adsorption on the Mo edge, where structures with molecular or atomic hydrogen adsorption are exothermic. This indicates the fundamental difference between S and Mo edges, and this is because Mo centers for hydrogenation adsorption are coordinatively unsaturated on the Mo edge but coordinatively saturated on the S edge. Nevertheless, the most stable adsorption forms are structure **8** with two –SH groups on the S edge and structure **7** with one –SH and one –MoH at the intersection of both Mo and S edges.

Lots of efforts also have been devoted to clarify the process of H spillover. In the remote control theory, Delmon et al. [6] proposed that promoter (Co, Ni) could accelerate the

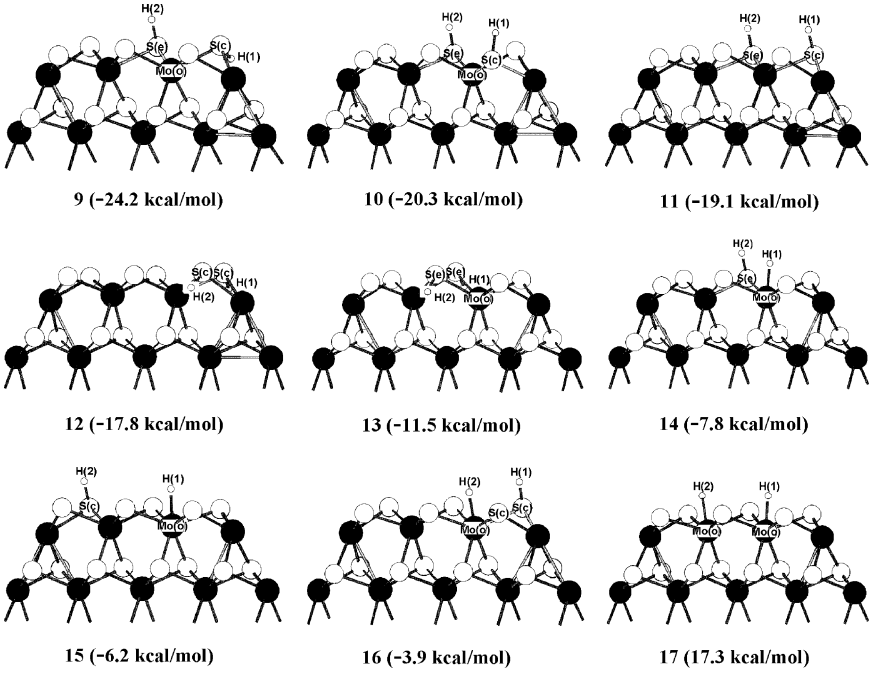

Fig. 4. H adsorption modes (**9**–**17**) and adsorption energies on the S edge.

dissociation of adsorbed H_2 effectively into atomic hydrogen, which can migrate to the active phase and create active sites. It is well known that spillover displays a powerful explanatory ability associated with the capability to be a very useful operating tool for the design of multi-component catalytic systems [60], as those generally encountered in heterogeneous catalysis. This property of spillover is either of a static or dynamic nature. Due to the very small amounts of promoter needed, it is hard to characterize the detailed spillover process by experiments [61]. In other cases spillover species act as a true reactant responsible for the main catalytic reaction [61]. For this purpose, we have computed the mobility of the adsorbed surface hydrogen. The mobility of the surface hydrogen on the Mo edge, S edge and the intersection of Mo and S edges is discussed, respectively, and the potential energy surfaces are shown in Fig. 5.

As shown in Fig. 5a, the activation barrier from the more stable molecular hydrogen complex (**2**) to the more stable dissociated hydrogen complex (**3**) is only 6.2 kcal/mol, and the corresponding hydrogen transfer barrier from **4** to **3** is 8.1 kcal/mol. For comparison, we have calculated the activation barrier of hydrogen transfer from the Mo edge to the S edge. As shown in Fig. 5b, the barrier between **1** and **7** is 12.7 kcal/mol, and that between **5** and **7** is 17.0 kcal/mol.

Furthermore, the activation barriers of hydrogen transfer on the S edge are calculated. As shown in Fig. 5c, the largest activation barrier from **5** to **11** via intermediate **16** is 19.2 kcal/mol, and the corresponding barrier from **6** to **11** via intermediate **14** is only 13.2 kcal/mol. For structures **10** and **11** with small energy difference, the activation barrier of the mobility process is similar to that from **5** or **6**. Therefore, these rather lower barriers show the high mobility of the adsorbed hydrogen over the surface. All these indicate that hydrogen can migrate or walk freely on the catalyst surface under real reaction condition, and this will simplify further investigation in HYD and HDS processes.

For further comparison we have computed the frequencies for the most stable adsorption models on the Mo edge (**3** and **2**) and the S edge (**8**) as well as on the intersection (**7**). All these data are listed in Table 2, and data for the other less stable models are given for comparison. The stretching frequencies (ν) of **3** for Mo–H–Mo and Mo_e–H are 1275 and 2027 cm^{-1}, and their bending frequencies are 972 and 635 cm^{-1}, respectively, and there are also combined bending frequencies at 755 and 548 cm^{-1}. For **4**, the stretching frequency of activated H_2 is 2539 cm^{-1}, which is lower that that of free H_2 (calc. 4369 cm^{-1} and expt. 4401 cm^{-1}). On the intersection, the stretching frequencies of S_c–H and Mo_c–H for **7** are at 2662 and 2055 cm^{-1}, respectively, and the bending frequencies of S_c–H are at 649 and 514 cm^{-1}. On the S edge, the stretching frequencies of S–H of **8** are 2546 and 2556 cm^{-1}. The bending frequencies are in the range of 659–699 cm^{-1}.

Ratnasamy and Fripiat [62] have reported the S–H group frequencies (2640 and 2500 cm^{-1}) after adsorption of hydrogen on the MoS_2-pressed samples. The multiplicity of S–H bands was ascribed to the existence of different valence states of Mo cations including Mo^{4+}, Mo^{3+} and Mo^{2+} states. Jones et al. [63] also have observed the formation of S–H groups at 662 cm^{-1} after hydrogen dissociation on MoS_2. Hydrogen adsorption on

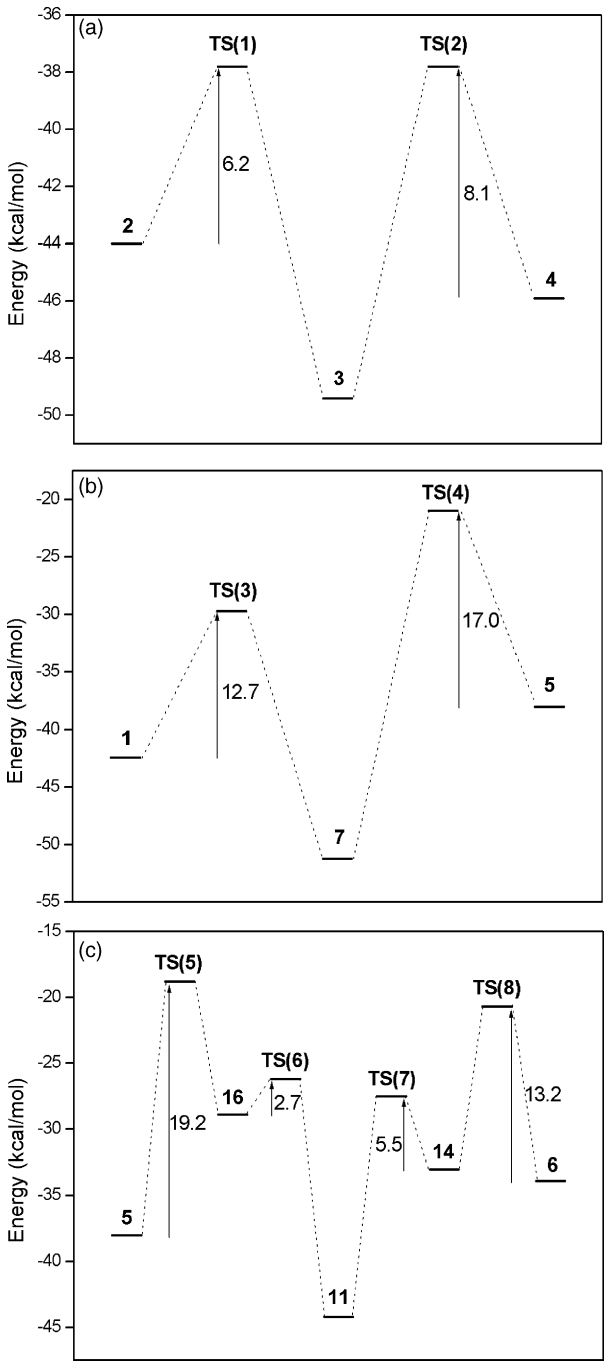

Fig. 5. Energy diagram of hydrogen migration: (a) on the Mo edge; (b) from the Mo edge to the S edge; (c) on the S edge.

MoS_2 was also investigated by inelastic neutron scattering [64], which shows strong band at 694 cm^{-1}, accompanied by weaker overtone maximums at 1380 and 2074 cm^{-1}, as well as by two more features at 2470 and 2679 cm^{-1} at 673 K. These latter two frequencies were reasonably attributed to the stretching modes of two kinds of S–H groups, similar to those observed in the IR spectra of MoS_2 [62]. The computed frequencies for S–H groups (2568–2662 cm^{-1} versus 500–769 cm^{-1}) and the available IR data (2640 and 2500 cm^{-1} versus 662 and 694 cm^{-1}) [62–64] show very good agreement. However, one has to consider this agreement with caution, this is because our model has only one

Table 2
The stretching (ν) and bending (δ) frequencies (cm^{-1}) for Mo–H and S–H

	Mode	Frequency		Mode	Frequency
1	ν_{H-H}	2910	**6**	$\nu_{sym(S-H)}$	2627
	$\nu_{sym(Mo(c)-2H)}$	898		$\nu_{asym(S-H)}$	2633
	$\nu_{asym(Mo(c)-2H)}$	1513		$\delta_{sym(S-H)}$	642, 536
	$\delta_{Mo(c)-2H}$	683, 470		$\delta_{asym(S-H)}$	564, 500
2	ν_{H-H}	2539	**7**	ν_{S-H}	2662
	$\nu_{sym(Mo(c)-2H)}$	1058		ν_{Mo-H}	2055
	$\nu_{asym(Mo(c)-2H)}$	1650		δ_{Mo-H}	769, 620
	$\delta_{Mo(c)-2H}$	755, 469		δ_{S-H}	649, 514
3	$\nu_{Mo(e)-H}$	2027	**8**	$\nu_{S(c)-H}$	2546
	$\nu_{Mo-H-Mo}$	1275		$\nu_{S(e)-H}$	2556
	$\delta_{Mo-H-Mo}$	972		$\delta_{S(c)-H}$	699, 679
	$\delta_{sym(Mo-H-Mo/Mo-H)}$	755		$\delta_{S(e)-H}$	691, 659
	$\delta_{asym(Mo-H-Mo/Mo-H)}$	548	**11**	$\nu_{S(c)-H}$	2615
	$\delta_{Mo(e)-H}$	635		$\nu_{S(e)-H}$	2647
4	$\nu_{Mo(c)-H}$	1956		$\delta_{S(c)-H}$	673, 525
	$\nu_{Mo(e)-H}$	1745		$\delta_{S(e)-H}$	683, 571
	$\delta_{Mo(c)-H}$	727	**14**	$\nu_{S(e)-H}$	2660
	$\delta_{Mo(e)-H}$	495		$\nu_{Mo(o)-H}$	1991
5	$\nu_{sym(S-H)}$	2568		$\delta_{S(e)-H}$	689, 570
	$\nu_{asym(S-H)}$	2587		$\delta_{Mo(o)-H}$	1027
	$\delta_{sym(S-H)}$	699, 560			
	$\delta_{asym(S-H)}$	611, 496			

H_2 adsorbed, and it differs from the experiments, in which multiple adsorptions are possible. This is discussed in the following section.

3.2. Adsorption at high hydrogen coverage

3.2.1. Adsorption on the Mo edge

In order to clarify coverage effects, we have calculated the hydrogen coverage of 100% (six hydrogen atoms) and 67% (four hydrogen atoms) on the Mo edge. The optimized adsorption structures are shown in Fig. 6, and **18** and **19** have 100% hydrogen coverage. In **18**, three H_2 probes are located germinally at two Mo_c and one Mo_e, and the H–H bond lengths are 0.820 and 0.854 Å, respectively. This shows that H_2 at Mo_e is more activated than that at Mo_c. Alike one H_2 adsorption (**1** and **2**), they are activated, but not dissociated, and represent the initial point for H_2 dissociation.

In **19**, there are two Mo–H–Mo bridge groups, two terminal Mo–H groups and two –SH groups. It represents the dissociated adsorption of H_2 on the Mo edge, and this is similar to those in **3** and **4** for one H_2 adsorption. As given in Table 1, the adsorption energy of **19** is higher than that of **18** (−66.6 kcal/mol versus −43.8 kcal/mol). The adsorption of dissociated hydrogen is more favored thermodynamically than the activated one at high coverage.

For 67% hydrogen coverage, there are five different structures (**20**–**24**) on the Mo edge. The two adsorbed H_2 molecules are located at one Mo_c site and one Mo_e site in **20**, while they are located at two Mo_c sites in **21**. The adsorption energies in Table 1 show that **20** has more activated H_2 than **21** (−31.4 kcal/mol versus −30.2 kcal/mol), and indicate in turn that the edge Mo atoms favor hydrogen adsorption thermodynamically more strongly than the corner Mo atoms. As shown in Fig. 6, the most stable **22** has three terminal Mo–H groups and one Mo–H–Mo bridge group within 67% hydrogen coverage, and the next most stable adsorption forms are structures **23** (0.2 kcal/mol) with two terminal Mo–H groups, one Mo–H–Mo bridge group and one –SH group, and **24** (2.3 kcal/mol) with three terminal Mo–H groups and one –SH group. It generally shows that the adsorption of dissociated hydrogen represents the more stable structures for hydrogen on the Mo edge, and this agrees well with the case of one H_2 adsorption.

The stretching frequencies of different Mo–H groups and activated H_2 are listed in Table 3. In **18**, **20** and **21**, the stretching frequencies of activated H_2 are lower that of free H_2 (calc. 4369 cm^{-1} and expt. 4401 cm^{-1}). In **19**, **22**–**24**, the stretching

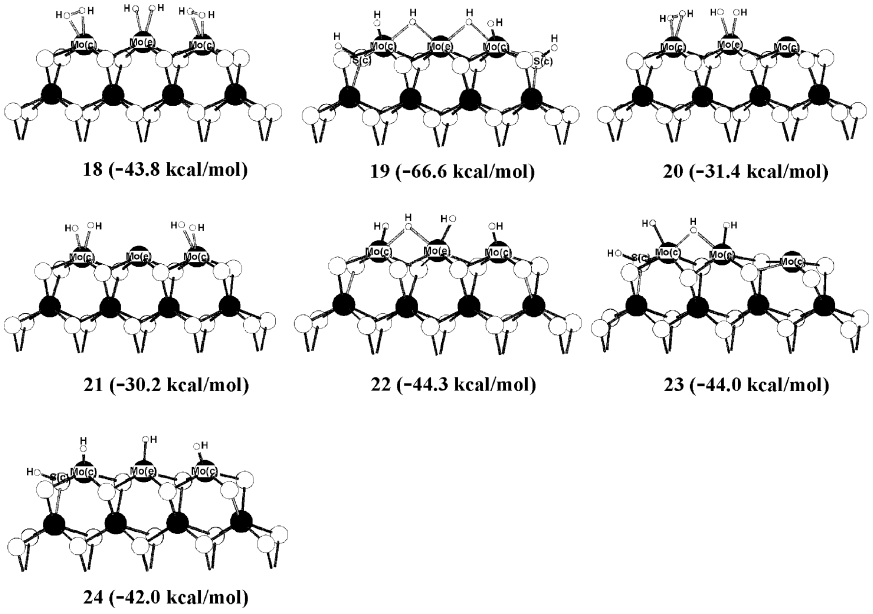

Fig. 6. The optimized structures **(18–24)** of multiple hydrogen adsorptions and adsorption energies on the Mo edge.

Table 3
The stretching (ν) and bending (δ) frequencies (cm^{-1}) for Mo–H and H–H

	Mode	Frequency		Mode	Frequency
18	ν_{H-H}	2818 (Mo_e)[a]	**22**	$\nu_{Mo(c)-H}$	1826
	ν_{H-H}	3263, 3239 (Mo_c)[b]		$\nu_{Mo(e)-H}$	1905, 1890
	$\nu_{Mo(c)-2H}$	1494, 1390		$\nu_{Mo-H-Mo}$	1337
	$\nu_{Mo(e)-2H}$	1522, 952		$\delta_{Mo-H-Mo}$	979, 786
19	ν_{S-H}	2634	**23**	ν_{S-H}	2657
	$\nu_{Mo(c)-H}$	2059, 1897		$\nu_{Mo(c)-H}$	1816
	$\nu_{Mo-H-Mo}$	1217, 1078		$\nu_{Mo(e)-H}$	2057
	$\delta_{Mo-H-Mo}$	1050, 910		$\nu_{Mo-H-Mo}$	1400
20	ν_{H-H}	2688 (Mo_e)	**24**	ν_{S-H}	2636
	ν_{H-H}	3278 (Mo_c)		$\nu_{Mo(c)-H}$	2105, 2087
	$\nu_{Mo(c)-2H}$	1567, 989		$\nu_{Mo(e)-H}$	1874
	$\nu_{Mo(e)-2H}$	1396, 837			
21	ν_{H-H}	2579 (Mo_c)			
	$\nu_{Mo(c)-2H}$	1087, 904			

[a] H_2 located at Mo_e.
[b] H_2 located at Mo_c.

Table 4
The stretching (ν) and bending (δ) frequencies (cm^{-1}) for S–H

	Mode	Frequency		Mode	Frequency
25	$\nu_{(Sc-H)D}$	2559, 2547	**28**	$\nu_{(Sc-H)D}$	2563, 2553
	$\nu_{(Se-H)D}$	2531, 2501		$\nu_{(Se-H)D}$	2580, 2560
	$\delta_{sym(Sc-H)D}$	706		$\delta_{sym(Sc-H)D}$	741, 715
	$\delta_{asym(Sc-H)D}$	685		$\delta_{asym(Sc-H)D}$	648, 636
	$\delta_{sym(Se-H)D}$	648		$\delta_{sym(Se-H)D}$	679
	$\delta_{asym(Sc-H)D}$	634		$\delta_{asym(Se-H)D}$	617
26	$\nu_{(Sc-H)D}$	2584, 2572	**29**	$\nu_{(Sc-H)D}$	2567, 2546
	$\delta_{sym(Sc-H)D}$	697, 637		$\delta_{sym(Sc-H)D}$	715, 705
	$\delta_{asym(Sc-H)D}$	673, 608		$\delta_{asym(Sc-H)D}$	630
27	$\nu_{(Sc-H)D}$	2570, 2558	**30**	$\nu_{(Sc-H)D}$	2539, 2505
	$\nu_{(Se-H)D}$	2569, 2544		$\nu_{(Se-H)D}$	2608, 2587
	$\delta_{sym(Sc-H)D}$	674, 655		$\delta_{sym(Sc-H)D}$	770
	$\delta_{asym(Sc-H)D}$	641, 621		$\delta_{asym(Sc-H)D}$	687
	$\delta_{sym(Se-H)D}$	635		$\delta_{sym(Se-H)D}$	667
	$\delta_{asym(Se-H)D}$	605		$\delta_{asym(Se-H)D}$	601

frequencies of terminal Mo–H groups and Mo–H–Mo groups are in the range of 1816–2087 and 1078–1400 cm^{-1}, in a good agreement with the stretching frequency difference between **1** and **2** with one H_2 adsorption in Table 2. Due to the frequency overlap of the terminal Mo–H groups, it should be hard to identify the frequencies of each terminal Mo–H group experimentally. However, it is certainly possible to identify the frequencies of terminal Mo–H groups (1816–2087 cm^{-1}) and Mo–H–Mo bridging groups (1078–1400 cm^{-1}).

3.2.2. Adsorption on the S edge

For further comparison, we have calculated the hydrogen coverage of 100% (six hydrogen atoms) and 67% (four hydrogen atoms) on the S edge. We have calculated two kinds of hydrogen adsorption with different orientations at high coverage. The optimized adsorption structures are shown in Fig. 7. For structure **25**–**30**, the –SH groups with the hydrogen atoms keeping away from the plane consisting of all Mo atoms are created, while in structures **28**–**30** the orientation of –SH gets closer to the plane consisting of all Mo atoms. Here the S–H groups are classified into two groups according to their character: double S_c–H group and double S_e–H group, which are symbolized by $(S_c–H)_D$, $(S_e–H)_D$, respectively.

As shown in Table 1, the adsorption energies of **25**, **26** and **27** are higher than those of **28**, **29** and **30**, respectively. This shows that the adsorption configuration with hydrogen atoms keeping away from the plane consisting of all Mo atoms is more stable. This is similar to the case of one H_2 adsorption in **8** and **10**, and they agree with those found from the periodic model calculations [35,38].

The stretching frequencies of different –SH groups are listed in Table 4. In **25**–**27**, the stretching frequencies of $(S_c–H)_D$ and $(S_e–H)_D$ groups are in the range of 2547–2584 and 2501–2569 cm^{-1}, respectively. In **28**–**30**, the stretching frequencies of $(S_c–H)_D$ groups (2505–2567 cm^{-1}) are lower than those of $(S_e–H)_D$ groups (2560–2608 cm^{-1}), and the difference is 55–59 cm^{-1}, which agree well with the stretching frequencies difference between structure **5** (2568–2587 cm^{-1}) and **6** (2627–2633 cm^{-1}) in Table 2. This shows that the frequencies of S–H will reduce with the increase in hydrogen coverage. The results show that all S–H groups stretching frequencies are in the experimentally observed region of 2500–2670 cm^{-1}, and the bending frequencies are in the region of 595–770 cm^{-1}. Due to the overlap of the S–H group frequencies, it is hard to identify the frequencies of individual S–H groups.

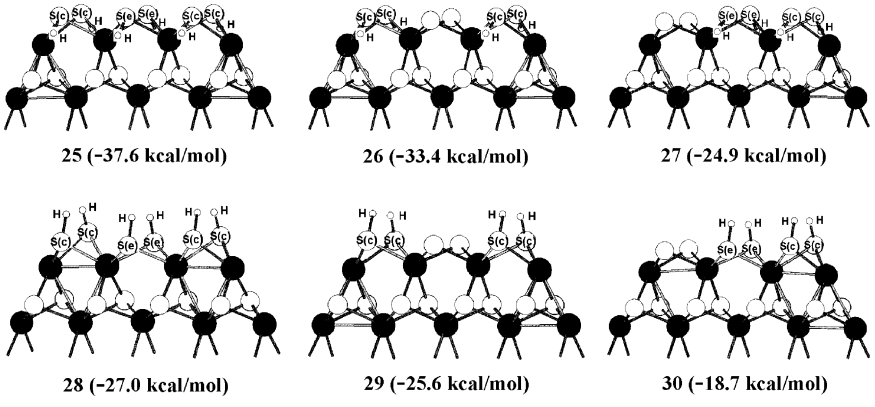

Fig. 7. The optimized structures **(25–30)** of multiple hydrogen adsorptions and adsorption energies on the S edge.

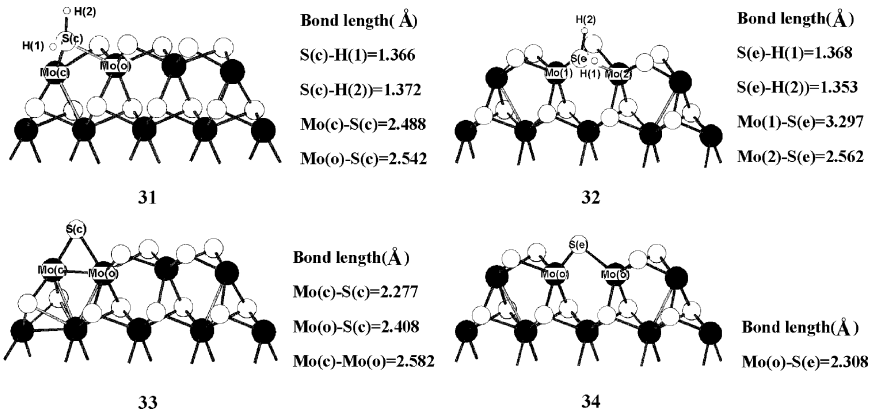

Fig. 8. Hydrogen adsorption on the S sites (**31** and **32**) and the formation of the reduced $Mo_{27}S_{53}$ clusters (**33** and **34**).

3.3. Formation CUS on the S edge

It has been suggested that –SH groups can develop by breaking a Mo–S–Mo linkage with hydrogen [1,9], which plays a crucial role in the HDS reaction. Ample experimental evidence corroborates the faculty of forming –SH groups over stoichiometry [10,18–22]. Furthermore, –SH groups are essential for the formation of CUS, which is proposed to be the active sites for HDS.

Recently, a study of scanning tunneling microscopy allowed the direct observation of the surface reaction *–SH + *–SH → * + H_2S proceeding during the hydrogenation of monolayer MoS_2 films by atomic hydrogen ($P = 10^{-9}$ Torr, $T = 600$ K) [45]. On the basis of these findings, it is necessary to study the mechanism of CUS formation on the S edges by molecular hydrogen and adsorbed H.

In our model, the removal of the S(c) and S(e) were chosen. Starting from $Mo_{27}S_{54}$, there are two possibilities to adsorb hydrogen with two germinal –SH bonds, as shown in Fig. 8. In structure **31**, the H_2S(c) group is at the corner of the S edge, while the H_2S(e) group in **32** is in the middle of the S edge, and the former is 2.1 kcal/mol more stable than the latter (Table 1). After the removal of H_2S, two $Mo_{27}S_{53}$ structures with newly created CUS on the corner (**33**) and in the middle of the S edge (**34**) are formed, and **33** is 15.3 kcal/mol more stable than **34**, respectively, indicating the preferred formation of CUS at the corner of the S edge thermodynamically; i.e., sulfur removal from corners is much easier than that from edges, and this different thermodynamic property validate the use of the cluster model, while models from periodic condition have only edges. This suggests that corners might play a key role in the catalytic process. This agrees with the previous result [65].

In addition, we have also calculated the formal reaction enthalpies. Eq. (2) represents the reduction of $Mo_{27}S_{54}$ cluster with the removal of S(c) to form $Mo_{27}S_{53}$ (**33**), and Eq. (3) the formation of $Mo_{27}S_{53}$ (**34**) with the removal of S(e), respectively. The rather thermal neutral reaction enthalpy of 0.7 kcal/mol in Eq. (2) indicates the potential ability of molecular H_2 to move sulfur at the corner of the S edge, while Eq. (3) is highly endothermic and the removal of sulfur in the middle of the S edge by H_2 is unlikely. On the basis of H_2 dissociation energy of 104.2 kcal/mol [58], it is expected that both types of sulfur can be removed by atomic hydrogen with highly exothermic reaction enthalpies of −104.6 and −83.9 kcal/mol. Our computational results correspond to the experimentally findings that H_2 cannot react directly with MoS_2 slabs under normal HYD/HDS conditions [66]. Therefore, the adsorbed hydrogen (or atomic hydrogen) on the S edges plays a very important role in creating CUS for HYD/HDS:

$$Mo_{27}S_{54} + H_2 \rightarrow Mo_{27}S_{53}(\mathbf{33}) + H_2S, \quad \Delta E = 0.7\,\text{kcal/mol} \tag{2}$$

$$Mo_{27}S_{54} + H_2 \rightarrow Mo_{27}S_{53}(\mathbf{34}) + H_2S, \quad \Delta E = 16.0\,\text{kcal/mol} \tag{3}$$

4. Conclusion

Hydrogen adsorption, dissociation and transfer as well as the formation of coordinatively unsaturated sites (CUS) on the surface of a singly slab $Mo_{27}S_{54}$ cluster have been computed at the level of density functional theory. On the surface of $Mo_{27}S_{54}$, there are S and Mo edges for hydrogen adsorption. The computed adsorption and relative energies have revealed that homolytic dissociation on the S edge with two S–H groups and heterolytic dissociation on the intersection of Mo and S edges with the formation of –SH and/or Mo–H bonds is more favored thermodynamically. The calculated frequencies of S–H agree well with experimental vibrational frequencies.

It has been computed that the adsorbed hydrogen on the $Mo_{27}S_{54}$ surface has enhanced mobility, as indicated by the rather low activation barriers for hydrogen dissociation and transfer processes. In agreement with the experiments, molecular hydrogen is not active enough for the removal of surface sulfur to create CUS, but atomic hydrogen is highly active. It is shown that sulfur removal from corner sites is much easier than that from edge sites. The thermodynamically more favored property of corner sites for hydrogen adsorption and formation of CUS validate the use of the cluster model, which is more realistic than the periodic model under the real reaction condition.

Despite the close agreement between computation and experiment, it is necessary to point out that the employed molecular systems for modeling the complicated real catalysts are approximated and limited. For example, the changes of surface structure and composition (like 0% Mo and 100% S) of MoS_2 are not taken into account. In addition, the degree and thermodynamic properties of cluster aggregations are very sensitive to the catalytic activity, and the roles of supports and promoters are very important to the catalytic properties. All these will direct our future work.

Acknowledgements

This work was supported by Chinese Academy of Science and the National Nature Foundation of China (20473111, 20590361 and 20573127).

References

[1] B. Delmon, G.F. Froment, Catal. Rev. Sci. Eng. 38 (1996) 69.
[2] H. Topsøe, B.S. Clausen, F.E. Massoth, in: J.R. Anderson, M. Boudart (Eds.), Hydrotreating Catalysis, Springer, Berlin, 1996.
[3] A.N. Startsev, Catal. Rev. Sci. Eng. 37 (1995) 353.
[4] R. Prins, V.H.J. De Beer, G.A. Somorjai, Catal. Rev. Sci. Eng. 31 (1989) 1.
[5] M. Daage, R.R. Chianelli, J. Catal. 149 (1994) 414.
[6] B. Delmon, Bull. Soc. Chim. Belg. 88 (1979) 979.
[7] B. Delmon, in: D.L. Trimm, S. Akashah, M. Absi-Halabi, A. Bishara (Eds.), Catalysts in Petroleum Refining. 1989, Elsevier, Amsterdam, 1990, p. 1.
[8] B. Delmon, Catal. Lett. 22 (1993) 1.
[9] Y.-W. Li, B. Delmon, J. Mol. Catal. A 127 (1997) 163.
[10] C.J. Wright, C. Sampson, D. Fraser, R.B. Moyes, P.B. Wells, C. Riekel, J. Chem. Soc., Faraday Trans. 176 (1980) 1585.
[11] J. Polz, H. Zeilinger, B. Müller, H. Knözinger, J. Catal. 120 (1989) 22.
[12] W.P. Dianis, Appl. Catal. 30 (1987) 99.
[13] A.B. Anderson, Z.Y. Al-Saigh, W.K. Hall, J. Phys. Chem. 92 (1988) 803.
[14] M.R. Dubois, M.C. van Der Veer, D.L. Dubois, R.C. Haltiwanger, N.K. Miller, J. Am. Chem. Soc. 102 (1980) 7456.
[15] J.C. Duchet, E.M. van Oers, V.H.J. de Beer, R. Prins, J. Catal. 80 (1983) 386.
[16] G.L. Schrader, C.P. Cheng, J. Catal. 80 (1983) 369.
[17] E. Payen, S. Kasztelan, J. Grimblot, J. Mol. Struct. 174 (1988) 71.
[18] P. Ratnasamy, J.J. Fripiat, J. Chem. Soc., Faraday Trans. 66 (1970) 2897.
[19] N.Y. Topsøe, H. Topsøe, J. Catal. 139 (1993) 641.
[20] H. Topsøe, B.S. Clausen, N.Y. Topsøe, J.K. Nørskov, C.V. Ovesen, C.J.H. Jacobsen, Bull. Soc. Chim. Belg. 104 (1995) 283.
[21] P. Sundberg, R.B. Moyes, J. Tomkinson, Bull. Soc. Chim. Belg. 100 (1991) 967.
[22] N.Y. Topsøe, H. Topsøe, F.E. Massoth, J. Catal. 119 (1989) 252.
[23] C. Petit, F. Maugé, J.C. Lavalley, Stud. Surf. Sci. Catal. 106 (1997) 157.
[24] G. Berhault, M. Lacroix, M. Breysse, F. Maugé, J.C. Lavalley, H. Nie, L. Qu, J. Catal. 178 (1998) 555.
[25] A. Travert, F. Maugé, Stud. Surf. Sci. Catal. 127 (1999) 269.
[26] J.V. Lauritsen, M. Nyberg, R.T. Vang, M.V. Bollinger, B.S. Clausen, H. Topsøe, K.W. Jacobsen, E. Lægsgaard, J.K. Nørskov, F. Besenbacher, Nanotechnology 14 (2003) 385.
[27] J.V. Lauritsen, M. Nyberg, J.K. Nørskov, B.S. Clausen, H. Topsøe, E. Lægsgaard, F. Besenbacher, J. Catal. 224 (2004) 94.
[28] C. Thomas, L. Vivier, J.L. Lemberton, S. Kasztelan, G. Pérot, J. Catal. 167 (1997) 1.
[29] C. Thomas, L. Vivier, M. Lescanne, S. Kasztelan, G. Pérot, Catal. Lett. 58 (1999) 33.
[30] C. Thomas, L. Vivier, A. Travert, F. Maugé, S. Kasztelan, G. Pérot, J. Catal. 179 (1998) 495.
[31] A. Scaffidi, L. Vivier, A. Travert, F. Maugé, S. Kasztelan, C. Scott, G. Pérot, Stud. Surf. Sci. Catal. 138 (2002) 31.
[32] E.J.M. Hensen, H.J.A. Brans, G.M.H.J. Lardinois, V.H.J. de Beer, J.A.R. van Veen, R.A. van Santen, J. Catal. 192 (2000) 98.
[33] M. Neurock, R.A. van Santen, J. Am. Chem. Soc. 116 (1994) 4427.
[34] F. Frechard, P. Sautet, Surf. Sci. 389 (1997) 131.
[35] S. Cristol, J.F. Paul, E. Payen, D. Bougeard, S. Clémendot, F. Hutschka, J. Phys. Chem. B 104 (2000) 11220.
[36] A. Travert, H. Nakamura, R.A. van Santen, S. Cristol, J.F. Paul, E. Payen, J. Am. Chem. Soc. 124 (2002) 7084.
[37] L.S. Byskov, M. Bollinger, J.K. Nørskov, B.S. Clausen, H. Topsøe, J. Mol. Catal. A 163 (2000) 117.
[38] M.V. Bollinger, K.W. Jaconben, J.K. Nørskov, Phys. Rev. B 67 (2003) 085410.
[39] Y.-W. Li, X.-Y. Pang, B. Delmon, J. Mol. Catal. A 169 (2001) 259.
[40] J.F. Paul, E. Payen, J. Phys. Chem. B 107 (2003) 4057.
[41] A.N. Startsev, J. Mol. Catal. A 152 (2000) 1.
[42] A. Müller, E. Diemann, A. Branding, F.W. Baumamm, M. Breysse, M. Vrinat, Appl. Catal. 62 (1990) L13.
[43] J.L. Brito, F. Severino, N.N. Delgado, J. Laine, Appl. Catal. A 173 (1998) 193.
[44] E. Diemann, T. Weber, A. Müller, J. Catal. 148 (1994) 288.
[45] S. Helveg, J.V. Lægsgaard, E. Lægsgaard, I. Stensgaard, J.K. Nørskov, B.S. Clausen, H. Topsøe, F. Besenbacher, Phys. Rev. Lett. 84 (2000) 951.
[46] C. Calais, N. Matsubayashi, C. Geantet, Y. Yoshimura, H. Shimada, A. Nishijima, M. Lacroix, M. Breysse, J. Catal. 174 (1998) 130.
[47] (a) B. Delley, J. Chem. Phys. 92 (1990) 508;
(b) B. Delley, J. Phys. Chem. 100 (1996) 6107;
(c) B. Delley, J. Chem. Phys. 113 (2000) 7756.
[48] J.P. Perdew, Y. Wang, Phys. Rev. B 45 (1992) 13244.
[49] Y.-W. Li, X.-Y. Pang, B. Delmon, J. Phys. Chem. A 104 (2000) 11375.
[50] H. Orita, K. Uchio, N. Itoh, J. Mol. Catal. A 195 (2003) 173.
[51] A.N. Startsev, V.I. Zaikovskii, Kinet. Katal. 35 (1994) 288.
[52] X. Ma, H.H. Schobert, J. Mol. Catal. A 160 (2000) 409.
[53] T. Zeng, X.-D. Wen, G.-S. Wu, Y.-W. Li, H. Jiao, J. Phys. Chem. B 109 (2005) 2846.
[54] T. Zeng, X.-D. Wen, Y.-W. Li, H. Jiao, J. Mol. Catal. A 241 (2005) 219.
[55] X.-D. Wen, T. Zeng, Y.-W. Li, J. Wang, H. Jiao, J. Phys. Chem. B 109 (2005) 18491.
[56] T. Shido, R. Prins, J. Phys. Chem. B 102 (1998) 8426.
[57] M.H. Farias, A.J. Gellman, G.A. Somorjai, R.R. Chianelli, K.S. Liang, Surf. Sci. 140 (1984) 181.
[58] S.J. Blanksby, G.B. Ellison, Acc. Chem. Res. 36 (2003) 255.
[59] W.K. Hall, W.S. Millman, Proceedings of the Seventh International Congress on Catalysis, Part B, Tokyo, 1980, p. 1304.
[60] G.M. Pajonk, in: G. Ertl, H. Knözinger, H. Weitkamp (Eds.), Handbook of Heterogeneous Catalysis, VCH, New York, 1997, p. 1064.
[61] C.M. Pajonk, Appl. Catal. A 202 (2000) 157.
[62] P. Ratnasamy, J. Fripiat, Trans Faraday Soc. 66 (1970) 2897.
[63] P.N. Jones, E. Knözinger, W. Langel, R.B. Moyes, J. Tomkinson, Surf. Sci. 207 (1989) 159.
[64] C.J. Wright, D. Fraser, R.B. Moyes, P.B. Wells, Appl. Catal. 1 (1981) 49.
[65] H. Schweiger, P. Raybaud, G. Kresse, H. Toulhoat, J. Catal. 207 (2002) 76.
[66] S.Y. Li, J.A. Rodriguez, J. Hrbek, H.H. Huang, G.-Q. Xu, Surf. Sci. 366 (1996) 29.